Article

Perfluoropropionic Acid (CF₃CF₂C(O)OH): Three Conformations and Dimer Formation

Carlos Omar Della Védova , Rosana Mariel Romano [*] , Hans Georg Stammler , Norbert W. Mitzel [*]

Article

Perfluoropropionic Acid (CF₃CF₂C(O)OH): Three Conformations and Dimer Formation

Carlos O. Della Védova, [1] **Rosana M. Romano,** [1,*] **Hans-Georg Stammler** [2] **and Norbert W. Mitzel** [2,*]

[1] Centro de Química Inorgánica "Dr. Pedro J. Aymonino", CEQUINOR (UNLP, CCT-CONICET La Plata, associated with CIC-PBA), Departamento de Química, Facultad de Ciencias Exactas, Universidad Nacional de La Plata, Boulevard 120 N° 1465, La Plata (CP 1900), Argentina

[2] Lehrstuhl für Anorganische Chemie und Strukturchemie, Center for Molecular Materials CM2, Bielefeld University, Universitätsstraße 25, 33615 Bielefeld, Germany

* Correspondence: romano@quimica.unlp.edu.ar; nmitzel@uni-bielefeld.de

Abstract: Perfluoropropionic acid (CF₃CF₂C(O)OH) will be investigated with a focus on its complex structural properties. As a formal derivative of propanoic acid, the incorporation of fluorine atoms imparts unique structural features, including three distinct monomeric conformations and a dimeric structure. This study presents experimental findings, supported by computational modeling, to explore these characteristics. The analysis includes an FTIR study of the isolated species in an Ar-cryogenic matrix and the low-temperature determination of its crystalline structure using single-crystal X-ray diffraction.

Keywords: Perfluoropropionic Acid; Low-Temperature Crystal Structure; Cryogenic Ar-Matrix Study; Conformers; Monomers; Dimer; Computational Calculations.

1. Introduction

The chemistry of fluorine has long been, and continues to be with renewed momentum, one of the most captivating fields for chemists worldwide. Fluorine, in its compounds, cannot be simply regarded as either a "larger hydrogen" or a "smaller chlorine." The properties of its compounds often prove to be unexpected, unpredictable, fascinating, and truly unique. For example, the energy transition has once again positioned fluorine at the forefront of the discipline. It is a key component of the salt used in lithium battery electrolytes, LiPF₆, and in its elemental form plays a vital role in chemically eliminating trace water by oxidizing it into OF₂ and HF [1].

In particular, fluoro- and perfluoro-organic compounds have found a wide range of applications. Specifically, perfluoroorganic compounds, one of which is the focus of this work, exhibit remarkable stability due to the presence of C-F bonds within their molecular structure. This stability—thermal, chemical, biological, and, to some extent, photochemical—confers upon them a significant degree of environmental persistence [2–13].

Perfluoropropionic acid, CF₃CF₂C(O)OH (PFPA), the title compounds, may not accumulate in the environment to the same extent as the longer chain perfluorinated carboxylic acids [7,8]; neither have its natural sources been identified so far. That it has been detected in rainwater [14–16], however, stresses its role as an environmentally active molecule. To fully understand how this and other long-lived products are formed under the complex environmental conditions present in a given reactive matrix, it is essential to acquire a detailed knowledge of the photochemical evolution of the species, their association equilibria at various temperatures, and to experimentally determine the existence of all conformers present at room temperature.

In the context of the anhydride molecule central to this study, it is worth noting that, from a structural perspective, the hydrate and dihydrate of perfluoropropionic acid were investigated using Chirped-Pulse Fourier Transform Microwave (CP-FTMW) Spectroscopy. The study revealed that the complexation of the −OH group of the acid with one or two water molecules occurs in the plane of the carboxylic acid group, resulting in the formation of a six- or eight-membered ring structure [17].

Important for this work is a vibrational study of $CF_3CF_2C(O)OH$ published by Crowder in 1972, in which he detailed the partial and total association of the species in the vapor and liquid states, respectively. The use of fundamental vibrational concepts, such as evaluating group electronegativity, allowed him to understand, for example, the shift to higher wavenumbers of the carbonyl stretch when a CF_3CF_2- group is formally replaced by a CF_3- group, and its connection with the hydrogen bonding comparison between the two species [18,19].

Another study explored the far-infrared spectra of a set of 27 carboxylic acids in aqueous solution, including the compound examined in this work. The analysis of the spectra, particularly in the OH stretching region, enables the determination of conformational isomerism [20]. Computational studies using DFT-B3LYP/6-311+G** and ab initio MP2/6-311+G** calculations on perfluoropropionic acid revealed the existence of an equilibrium between two conformations: the cis form (where the C=O group eclipses the C-C bond) and the gauche conformer. The calculations predict the *gauche*-conformer to be the lower-energy form at ambient temperature, with an abundance of 76% gauche and 24% cis at 298.15 K [21]. The structural properties of perfluoropropionic acid have been resolved through the study of its rotational spectrum using a pulsed nozzle, chirped-pulse Fourier transform microwave spectrometer in the frequency range of 8–14 GHz. According to the quantum-chemical calculations and spectral analysis, we conclude that the observed rotational isomer is the *gauche*-form, with the C−C−C=O dihedral angle predicted to be 106–107°, depending on the level of approximation used [22].

In another work, the chemistry of perfluoropropionic acid and its close derivatives was studied, described, and compared [23]. Perfluoropropionic acid was also included in an early study utilizing neutron spectroscopy to examine its vibrational spectrum, alongside a broader group of related organic acids [24]. The title compound was also investigated using gas-phase mid-IR, near-IR, and visible vibrational spectroscopy, alongside perfluorooctanoic and perfluorononanoic acid, employing Fourier transform and cavity ring-down spectroscopy. The authors of this work concluded that these compounds exhibit more harmonic O-H bonds, lower transition wavenumbers, and reduced intensities compared to shorter-chain hydrocarbon acids, alcohols, and peroxides [25]. The vibrational spectra of the title compound have also been presented in the range of 11,000–1,000 cm^{-1} and compared with those of its hydrocarbon homolog, propionic acid [26]. Perfluoropropionic acid was one of the compounds used to study a simple drop-coating deposition using Raman spectroscopy methods to concentrate perfluoroalkyl substances and subsequently design an accessible and reliable spectral library [27].

The family of polyfluorinated compounds, including $CF_3CF_2C(O)OH$, was analyzed from the perspective of the fragmentation process of the deprotonated species. It was indicated that the relative energy of the transition state of the formed CCFC ring, which leads to the FCO_2^- anion, is directly linked to the subsequent dissociation observed [28]. In another previous work we also employed perfluoropropionic acid to study details related to its photoexcitation, photoionization, and photofragmentation using synchrotron light energies in the range between 11.7 and 715.0 eV. At low energies, the detected fragments were COH^+, $C_2F_4^+$, and the parent M^+ ion. In this work, and in line with the experimental variables used—for instance, very low pressures on the order of 10^{-6} mm Hg—there was no evidence of the existence of a dimer of perfluoropropionic acid [29].

$CF_3CF_2C(O)OH$ has also been part of a very recent study that evaluates the decomposition products of this family of compounds in research aimed at providing more information about the thermal evolution process [30]. In this context, and in connection with this evidence, the degradation of perfluoropropionic acid and related compounds was investigated using an argon plasma under various conditions [31].

A previous analysis of this type reports that after decomposition in an N_2 atmosphere at temperatures between 200 and 780 °C, the identified products are $CF_2=CF_2$, CF_3CF_2H, and $CF_3C(O)F$. In an O_2 atmosphere below 400 °C, the main product is OCF_2, accompanied by the inevitable formation of SiF_4 due to the use of a quartz reactor [32]. From a computational perspective, and to understand the transport behavior over considerable distances of relatively stable substances such as perfluoroalkyl and polyfluoroalkyl compounds, this work aims to comparatively determine the gas-phase thermochemical properties of the compounds, which includes perfluoropropionic acid [33]. The use of perfluoropropionic acid in studying its role in driving the nucleation of atmospheric molecules under ambient conditions is computationally analyzed to understand, at a molecular level, the composition and formation mechanism of secondary organic aerosols [34].

To fully comprehend how this and other long-lived products are formed under the intricate environmental conditions present in a given reactive matrix, it is crucial to gain a detailed understanding of the photochemical evolution of the species, their association equilibria at various temperatures, and to experimentally confirm the existence of all conformers present at room temperature. This comprehensive approach ensures a deeper insight into the mechanisms and interactions that drive the formation and stability of these products.

2. Results and Discussion

2.1. Quatum-Chemical Calculations

2.1.1. Monomer

With the aim of determining which conformations of $CF_3CF_2C(O)OH$ coexist in the gas phase at room temperature, a potential energy surface was calculated as a function of the dihedral angles $\varphi(C-C-C=O)$ and $\varphi(O-C-O-H)$ using the B3LYP/6-311+G(D) approximation (Figure S1).

The *gauche−syn*, *gauche−anti*, and *syn−syn* conformations (Figure 1) correspond to minima on the aforementioned potential energy surface, while the *syn−anti* structure corresponds to a saddle point. This represents a notable difference between $CF_3CF_2C(O)OH$ and its hydrogenated analog, which admits four stable conformations. Despite the stability of three $CF_3CF_2C(O)OH$ conformations, only one (*gauche−syn*) has been properly detected experimentally and studied.

The structures corresponding to the three mentioned conformers were optimized, and their harmonic vibrational frequencies were calculated using different approximations. Table 1 presents the values of the dihedral angles $\varphi(C-C-C=O)$ and $\varphi(O-C-O-H)$ for the different conformations, their relative energies, and their populations determined using the Boltzmann equation at room temperature, taking into account the double degeneracies for the gauche species due to symmetric considerations.
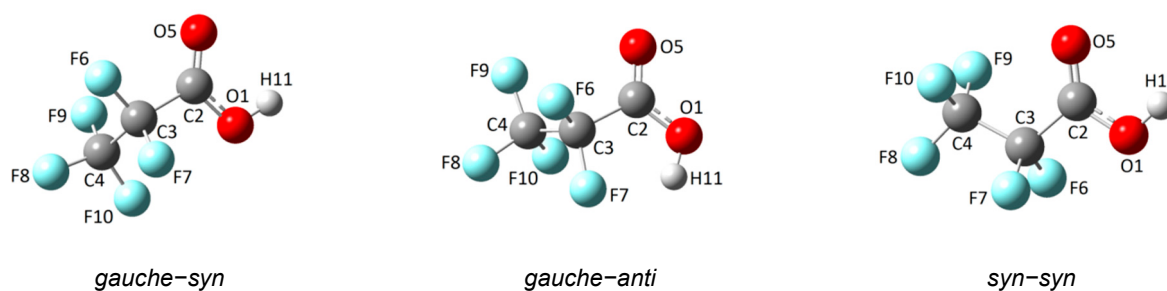

| | gauche−syn | gauche−anti | syn−syn |

Figure 1. Optimized structures (MP2/6-311+G(D)) of the *gauche−syn*, *syn−syn*, and *gauche−anti* conformers of $CF_3CF_2C(O)OH$.

Table 1. Energy and Gibbs free energy differences among *gauche−syn*, *gauche−anti*, and *syn−syn* conformers of $CF_3CF_2C(O)OH$, dihedral angles $\varphi(C-C-C=O))$ and $\varphi(O-C-O-H)$, and conformational population χ calculated at 298 K using the MP2/6-311+G(D) approximation.

Conformer	φ(C–C–C=O)	φ(O–C–O–H)	ΔE (kcal/mol)	ΔG (kcal/mol)	χ (%)
gauche–syn	101.2	−0.3	0.00	0.00	85.1
syn–syn	−0.1	0.0	0.43	0.62	14.7
gauche–anti	82.3	176.6	3.37	3.64	0.2

2.1.2. Dimer

The structure of the $CF_3CF_2C(O)OH$ dimer (Figure 2) was calculated using the MP2/6-311+G(D) approximation, taking into account that the structure determined by X-ray diffraction reproduces these data (see X-ray diffraction section). The dimer consists of two enantiomeric monomeric units (*gauche–syn*) properly oriented and linked to each other through two hydrogen bonds.
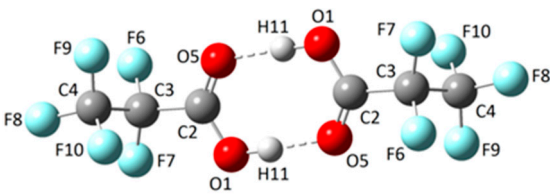

Figure 2. Optimized structures (MP2/6-311+G(D)) of the dimer of $CF_3CF_2C(O)OH$.

2.2. Experimental Results

2.2.1. Gas-Phase FTIR Spectra

In 1972, Crowder reported for the first time the infrared spectrum of the gas and liquid phases of $CF_3CF_2C(O)OH$ [18]. The FTIR spectrum of $CF_3CF_2C(O)OH$ in the gas phase shows evidence of the coexistence of three monomeric and one dimeric species (Figures 3 and 4). However, despite the good resolution of the acquired spectra (0.5 cm^{-1}), the different conformational contributions of the monomers remain unclear. The infrared spectrum assignment is detailed in Table S1.
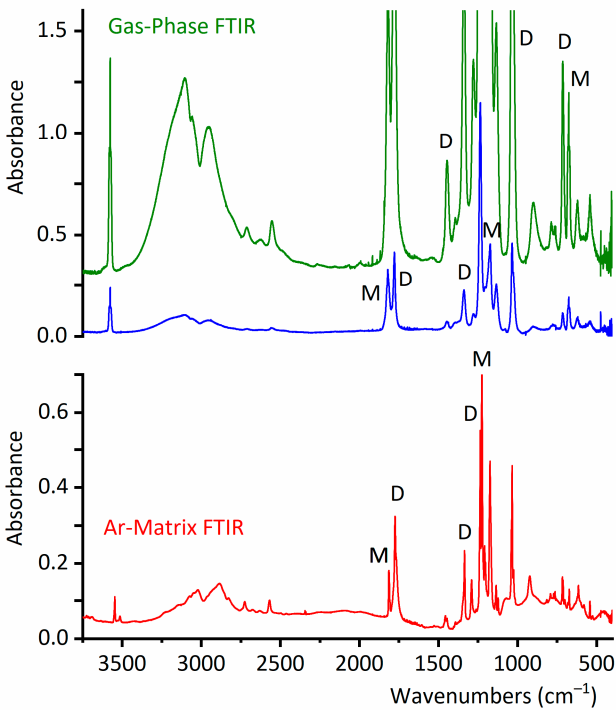

Figure 3. Gas-phase FTIR spectra of $CF_3CF_2C(O)OH$ (optical path 10 cm, resolution 0.5 cm^{-1}, pressure: 40 torr (top, green-trace) and 8 torr (middle, blue-trace) and Ar-matrix FTIR spectrum (bottom, red-trace) in $CF_3CF_2C(O)OH$:Ar 1:500 ration and resolution 0.5 cm^{-1}, in the 3740-400 cm^{-1} wavenumber region. Some of the bands of monomer and dimer species are indicated by M and D, respectively.
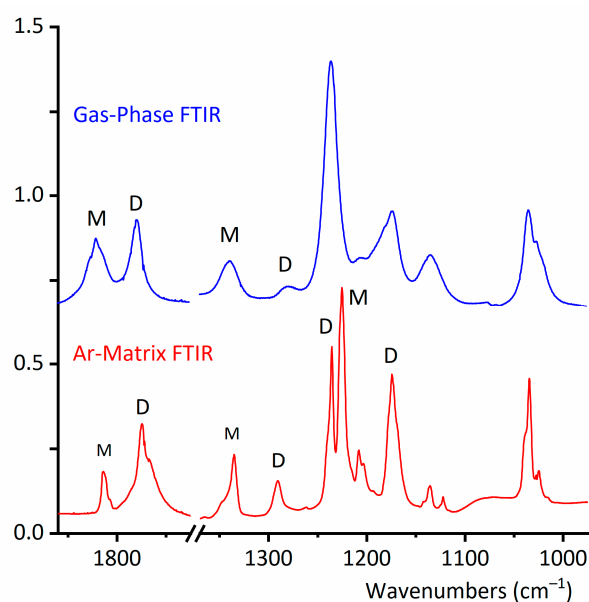
Figure 4. Selected regions of the gas-phase FTIR spectrum of CF₃CF₂C(O)OH (optical path 10 cm, resolution 0.5 cm⁻¹, pressure: 8 torr (top, blue-trace) and Ar-matrix FTIR spectrum (bottom, red-trace) in CF₃CF₂C(O)OH:Ar 1:500 ratio and resolution 0.5 cm⁻¹. Some of the bands of monomer and dimer species are indicated by M and D, respectively.

Next, the coexistence of monomers and a dimer of $CF_3CF_2C(O)OH$ will be confirmed through experiments conducted in the vapor phase. It is important to have this information to ensure that, during the preparation of the $CF_3CF_2C(O)OH$ matrix in Ar for deposition and measurement at cryogenic temperature, the dimer concentration is minimized. Figure 3 shows a selected section of the FTIR spectra in the vapor phase for $CF_3CF_2C(O)OH$ samples measured at different temperatures. In this region, two distinct bands clearly appear: one at 714 cm⁻¹, corresponding of the dimer, and another at 676 cm⁻¹, corresponding to the O-C=O bending of the *gauche-syn*-monomer. Figures 5 and 6 describe the results of experiments conducted with the vapor phase of the species, aiming to determine the optimal experimental conditions for ensuring that monomeric species predominate over the dimer in the matrix isolation experiments of perfluoropropionic acid.
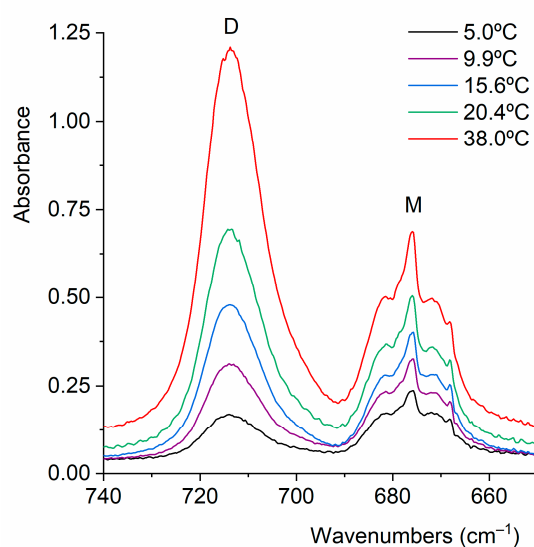

Figure 5. Gas-phase FTIR spectra of CF₃CF₂C(O)OH (optical path: 10 cm, resolution: 0.5 cm⁻¹) recorded from the liquid phase at different temperatures.
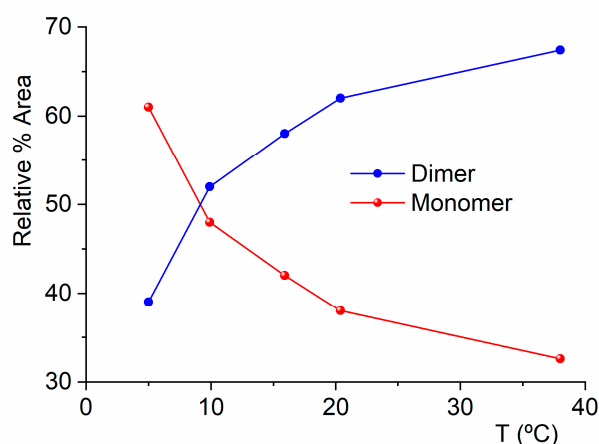
Figure 6. Relative percentage areas of the IR bands at 714 cm^{-1}, arising from the bending vibration of the O−C=O group in the dimeric CF$_3$CF$_2$C(O)OH species, and at 676 cm^{-1}, corresponding to the same mode in the monomeric acid in its *gauche-syn* conformation, as a function of the liquid temperature in equilibrium with the vapor phase.

2.2.2. FTIR Spectrum of CF$_3$CF$_2$C(O)OH Isolated in Solid Ar

The study of species isolation using cryogenic matrices enhances the resolution of infrared spectra by eliminating the contributions of rotational broadening at low temperatures, typically around 15 K. Thus, the infrared spectrum of the CF$_3$CF$_2$C(O)OH:Ar (1:500) matrix reveals the contributions of the *gauche−syn*- and *syn−syn*-conformers of CF$_3$CF$_2$C(O)OH, which coexist in the gas phase, but does not show the contribution of the *gauche−anti*-conformer, which is less abundant. This represents a difference between propionic acid, CH$_3$CH$_2$C(O)OH, and its perfluorinated counterpart: the matrix FTIR spectrum of the propionic acid at low temperatures only shows the existence of a single conformer [35]. Figure 4 compares the FTIR spectra of CF$_3$CF$_2$C(O)OH in the gas phase and in the matrix, highlighting the respective conformational contributions in the latter.

2.2.3. Matrix FTIR Spectra of CF$_3$CF$_2$C(O)OH after Broadband UV-VIS Irradiation

The matrix of CF$_3$CF$_2$C(O)OH diluted in argon in a 1:500 ratio at cryogenic temperatures was exposed to UV-vis broadband irradiation in the range of $200 \leq \lambda \leq 800$ nm. Spectra were acquired before irradiation and at different irradiation times (0.5, 1.5, 3, 6, 12, 30, and 60 min). The irradiation resulted in a decrease of the population of the lowest energy and most abundant conformer in the gas phase, the *gauche-syn*-conformer, and an increase in the *syn-syn*-conformer and the dimeric species. A significant finding was that after 30 min of irradiation, signals of the *gauche-anti* form appeared in the spectrum. This conformer had previously been elusive due to its relatively low concentration in the gas phase at room temperature. Thus, we obtained the first experimental evidence for the existence of this conformer. Figure 7 depicts the FTIR spectra of CF$_3$CF$_2$C(O)OH isolated in Ar, recorded immediately after deposition and after 60 min of broad-band irradiation in the carbonyl stretching vibrational region, which is highly sensitive to conformation. For clarity, the spectra were normalized to the carbonyl absorption of the lowest-energy conformer, the *gauche-syn*-rotamer.
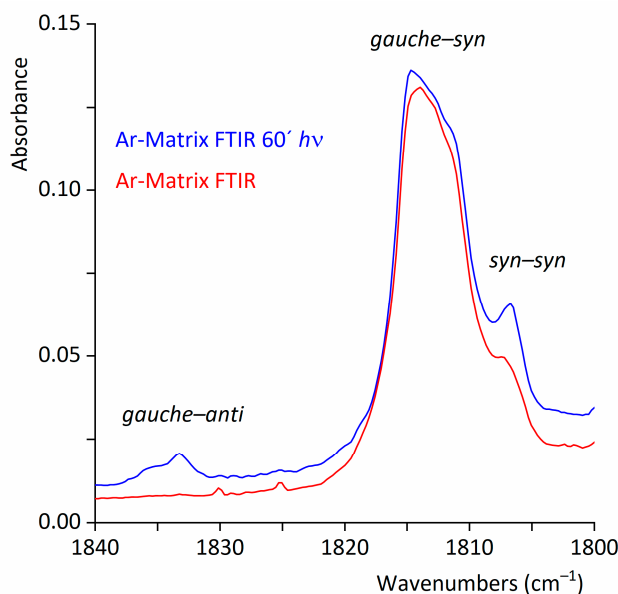
Figure 7. Ar-matrix FTIR spectra of $CF_3CF_2C(O)OH$ (resolution 0.5 cm^{-1}, $CF_3CF_2C(O)OH$:Ar 1:500 ratio) between 1840 and 1800 cm^{-1} taken immediately after deposition (bottom, red-trace) and after 60 min of broad-band UV-vis irradiation (top, blue-trace).

Figure 8 shows the variation in absorbance, measured as the integrated area of the IR bands, as a function of irradiation time. The features assigned to the *syn-syn*-form increase at the expense of the bands corresponding to the *gauche-syn*-rotamer. Additionally, the absorptions of the dimer also increase upon photolysis, presumably due to some monomer diffusion during irradiation.
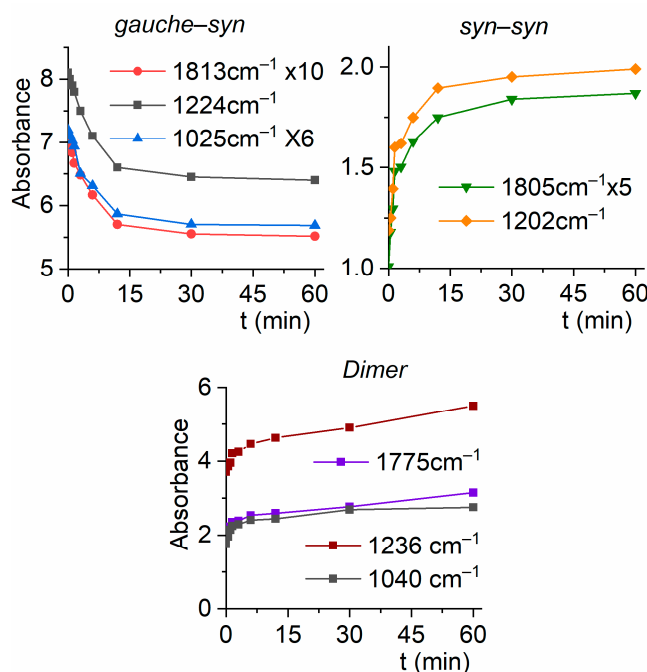
Figure 8. Absorbances of the IR bands of the $CF_3CF_2C(O)OH$:Ar (1:500) matrix for the *gauche-syn* (top left) and *syn-syn* (top right) conformers, as well as for the dimer (bottom), as a function of irradiation time.

2.2.4. Solid State Structure

The solid-state structure of CF3CF2C(O)OH has been studied from an in situ grown crystal. $CF_3CF_2C(O)OH$ crystallizes in the space group $P2_1/c$, forming dimers in which both monomers adopt a *gauche-syn* conformation, related to each other by a crystallographic center of inversion (Figure 9).

Table S2 presents crystallographic information obtained from the structural analysis and refinement of $CF_3CF_2C(O)OH$.
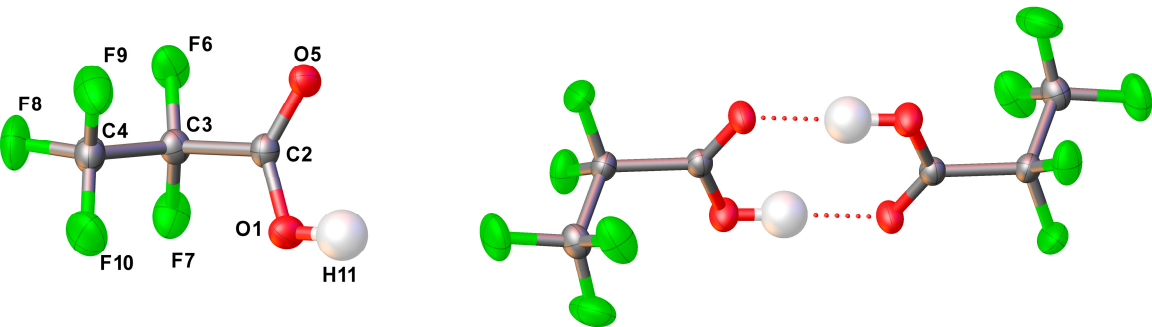

Figure 9. Left: Structure of CF_3CF_2COOH in the solid state. Thermal ellipsoids are shown at a probability level of 50%. Right: Dimer of CF_3CF_2COOH, symmetry code used: -X,1-Y,-Z.

The geometric parameters of $CF_3CF_2C(O)OH$ obtained by X-ray diffraction are listed below in Table 2, where they are compared with the values obtained by quantum-chemistry calculations showing that the calculated values reproduce the experimentally obtained fairly well, even though the computational values would be closer to those determined in the gas phase due to their intrinsic nature.

Table 2. Experimental parameters obtained by X-ray diffraction and computed parameters (distances in Å, angles in degrees) corresponding to the *gauche–syn*-conformer of $CF_3CF_2C(O)OH$.

Parameter	X-ray diffraction	MP2/6-311+G(D)
r F6−C3	1.338(2)	1.344
r F7−C3	1.336(2)	1.351
r F9−C4	1.319(2)	1.336
r F8−C4	1.317(2)	1.330
r F10−C4	1.304(2)	1.332
r O5=C2	1.215(2)	1.203
r O1−H11	0.97(3)	0.971
r O1−C2	1.286(2)	1.337
r C2−C3	1.545(2)	1.542
r C4−C3	1.542(2)	1.542
α H11−O1−C2	112.6(17)	108.3
α O5−C2−O1	127.9(2)	126.9
α O5−C2−C3	120.0(2)	123.0
α O1−C2−C3	112.0(2)	110.0
α F9−C4−F8	108.9(2)	109.0
α F9−C4−F10	108.8(2)	108.8
α F9−C4−C3	109.4(2)	109.4
α F8−C4−F10	109.1(2)	108.9
α F8−C4−C3	110.1(2)	110.1
α F10−C4−C3	110.6(2)	110.5
α F6−C3−C7	108.7(2)	108.9
α F6−C3−C2	109.0(2)	108.8
α F6−C3−C4	108.1(2)	107.7
α F7−C3−C2	110.5(2)	110.6
α F7−C3−C4	107.9(2)	108.0
α C2−C3−C4	112.6(2)	112.8
τ H11−O1−C2−O5	−0.5(18)	−0.3

τ H11−O1−C2−C3	−178.2(17)	178.8
τ O5−C2−C3−F6	21.2(2)	−18.2
τ O5−C2−C3−F7	140.6(2)	−137.8
τ O5−C2−C3−C4	−98.7(2)	101.2
τ O1−C2−C3−F6	−160.9(2)	162.6
τ O1−C2−C3−F7	−41.5(2)	43.1
τ O1−C2−C3−C4	79.2(2)	−78.0
τ F9−C4−C3−F6	−65.5(2)	65.1
τ F9−C4−C3−F7	177.2(2)	−177.4
τ F9−C4−C3−C2	54.9(2)	−54.9
τ F8−C4−C3−F6	54.1(2)	−54.7
τ F8−C4−C3−F7	−63.3(2)	62.8
τ F8−C4−C3−C2	174.5(2)	−174.7
τ F10−C4−C3−F6	174.7(2)	−175.0
τ F10−C4−C3−F7	57.3(2)	−57.6
F10−C4−C3−C2	−64.9(2)	65.0

According to NBO quantum-chemical calculations at the B3LYP/6-311+G(D) level of the theory, the aforementioned hydrogen bonds, which are responsible for dimer formation, arise from electronic transfer from a lone pair of the carbonyl oxygen to the anti-bonding molecular orbital $\sigma^*(O-H)$. This interaction leads to a second-order perturbation stabilization energy $E^{(2)}$ of 9.20 kcal/mol.

The hydrogen bond H11···O5 (symmetry code -X,1-Y,-Z) has a length of 1.70(3) Å, and the distance O1···O5 is 2.665(2) Å. Additionally, the only appreciable distance below the van der Waals distance (rvdW) [36] is the contact F6···C2 (symmetry code: +X,3/2-Y,1/2+Z) with 3.113(2) Å. However, the stabilization energy calculated for these interactions is not appreciable.

3. Materials and Methods

3.1. $CF_3CF_2C(O)OH$

The $CF_3CF_2C(O)OH$ 97 % was purchased from Sigma Aldrich and subsequently purified by distillation through a series of U-shaped cold traps immersed in cold baths at −50, −80, and −110°C, respectively.

3.2. Quantum-Chemical Calculations

The Gaussian 03 program [37] was used to perform quantum-chemical calculations, including the calculation of the potential energy function potential energy function for a specific dihedral angle, followed by geometry optimization of the corresponding minima and the calculation of their harmonic frequencies. For these purposes, the DFT [38] and MP2 [39] methods were chosen in conjunction with the 6-311+G(D) basis set. NBO [40] calculations were performed with the NBO 5.G package [41] incorporated in Gaussian 03. Additionally, the dimeric structure was computed using Gaussian 03. In this case, a potential energy curve was generated, followed by the optimization of the obtained minimum, employing the B3LYP/6-311+G(D) level of approximation.

3.3. Infrared Spectroscopy

Infrared spectra were recorded using a Nicolet™ 6700 spectrometer with a double-wall cell featuring a 10 cm optical path length and 0.5 mm thick Si windows. The spectral resolution was 0.5 cm⁻¹, and each spectrum was obtained by averaging 64 scans. To optimize the equilibrium between monomers and dimers of perfluoropropionic acid in the matrix study at cryogenic temperatures, spectra were recorded at various temperatures (5.0, 9.9, 15.6, 20.4, and 38.0°C) to determine the best experimental conditions.

3.4. Matrix Isolation Experiments

The gas mixture was deposited on a 15 K CsI window using the pulse deposition technique [42–44]. Low temperatures were achieved using a Displex closed-cycle refrigerator (SHI-APD Cryogenics, model DE-202). The corresponding FTIR spectra were acquired with the previously described instrument. A Spectra-Physics Hg-Xe arc lamp operating at 1000 W was used to irradiate the matrix within the 200–800 nm broad band range. To prevent matrix heating, a water filter was placed between the lamp and the matrix. Several spectra were recorded at different irradiation times.

3.5. X−Ray Diffraction Analysis

A single crystal of $CF_3CF_2C(O)OH$ was grown in situ within a capillary. The sample was filled into a capillary, cooled with liquid nitrogen forming a polycrystalline material. At 180 K a solid-liquid equilibrium near the melting point was established by melting the solid, leaving only a tiny crystal seed intact, using a thin copper wire as an external heat source. The temperature was then gradually lowered with 1 K/h to 176 K where the entire capillary was filled with crystalline specimen, followed by cooling to 146 K at a rate of 44 K per hour.

The crystal was maintained at 146.0(1) K during data collection, which was performed using an Agilent SuperNova diffractometer at Bielefeld University. Using Olex2 [45] the structure was solved by direct methods with SHELX-97 [46], and the refinement was carried out using Olex2.refine [47] and spherical scattering factors calculated with NoSpherA2 [48].

3. Conclusions

The evaluation of the results obtained through various spectroscopic techniques—vibrational IR, matrix IR spectra with UV-Vis broad band irradiation, as well as X-ray diffraction analysis—provide complementary data that allow for the study of conformations and equilibria in different families. It is worth noting that conformational properties are crucial for understanding the chemical behaviour of macromolecules and are responsible for the fundamental chemical behaviour of biological molecules [49,50].

In the present case, and in relation to the above-mentioned, the structure of $CF_3CF_2C(O)OH$, its dimer, and the existence of three conformations in equilibrium in the vapor phase have been conclusively determined. It is worth noting that the accurate assessment of the number of real conformers is a key tool for precisely approximating the electronic spectra of molecules. A purely computational approach requires evaluating thousands of geometries. In the recently published study, this computational effort is drastically reduced by using effective conformers for the calculation of UV-Vis spectra [51].

Supplementary Materials: The following supporting information can be downloaded at the website of this paper posted on Preprints.org, Figure S1: Potential energy surface of $CF_3CF_2C(O)OH$ as a function of the dihedral angles φ(O−C−O−H) and φ(C−C−C=O), displayed from different perspectives.; Table S1: Comparison between experimental and computed IR vibrational modes for $CF_3CF_2C(O)OH$ and their proposed assignment; Table S2: Crystallographic information for $CF_3CF_2C(O)OH$.

Author Contributions: All authors contributed to the results presented in this manuscript. In particular, H.-G.S. was responsible for the crystal structure resolution of the studied species.

Data Availability Statement: The original contributions presented in this study are included in the article/supplementary material. Further inquiries can be directed to the corresponding author.

References

1. Susarla N.; Ahmed, S. Estimating cost and energy demand in producing lithium hexafluorophosphate for Li-ion battery electrolyte, *Ind. Eng. Chem. Res.* **2019,** *58(9),* 3754−3766.
2. Moody, C.A.; Martin, J.W.; Kwan, W.C.; Muir, D.C.G.; Mabury, S.A. Monitoring perfluorinated surfactants in biota and surface water samples following an accidental release of fire-fighting foam into Etobicoke Creek. *Environ. Sci. Technol.* 2002, *36*, 545−551.
3. Zhang, C.; Yan, H.; Li, F.; Zhou, Q. Occurrence and fate of perfluorinated acids in two wastewater treatment plants in Shanghai, China. *Environ. Sci. Pollut. Res.* **2015**, *22*, 1804−1811.
4. Yamashita, N.; Kannan, K.; Taniyasu, S.; Horii, Y.; Petrick, G.; Gamo, T. A global survey of perfluorinated acids in oceans. *Mar. Pollut. Bull.* **2005**, *51*, 658−68.
5. So, M.K.; Miyake, Y.; Yeung, W.Y.; Ho, Y.M.; Taniyasu, S.; Rostkowski, P. Perfluorinated compounds in the Pearl River and Yangtze River of China. *Chemosphere*. **2007**, *68*, 2085−2095.
6. Ellis, D.A.; Mabury, S.A.; Martin, J.W.; Muir, D.C.G. Thermolysis of fluoropolymers as a potential source of halogenated organic acids in the environment. *Nature*. **2001**, *412*, 321−324.
7. Tian, Y.; Yao, Y.; Chang, S.; Zhao, Z.; Zhao, Y.Y.; Yuan, X.J.; Wu, F.C.; Sun, H.W. Occurrence and phase distribution of neutral and ionizable per- and polyfluoroalkyl substances (PFASs) in the atmosphere and plant leaves around landfills: A case study in Tianjin, China. *Environ. Sci. Technol.* **2018**, *52*, 1301−1310.
8. Martin, J.W.; Mabury, S.A.; Solomon, K.R.; Muir, D.C.G. Dietary accumulation of perfluorinated acids in juvenile rainbow trout (Oncorhynchusmykiss). *Environ. Tox. Chem.* **2003**, *22*, 189−195.
9. Martin, J.W.; Mabury, S.A.; Solomon, K.R.; Muir, D.C.G. Bioconcentration and tissue distribution of perfluorinated acids in rainbow trout (Oncorhynchusmykiss). *Environ. Tox. Chem*. **2003**, *22*, 196−204.
10. U.S. Environmental Protection Agency. Preliminary risk assessment of the developmental toxicity associated with exposure to perfluorooctanoic acid and its salts. Office of Pollution Prevention and Toxics, RiskAssessment Division, **2003**.
11. Berthiaume, J.; Wallace, K.B. Perfluorooctanoate, perflourooctanesulfonate, and N-ethyl perfluorooctanesulfonamido ethanol; peroxisome proliferation and mitochondrial biogenesis. *Toxicol. Lett.* **2002**, *129*, 23−32.
12. Upham, B.L.; Deocampo, N.D.; Wurl, B.; Trosko, J.E. Inhibition of gap junctional intercellular communication by perfluorinated fatty acids is dependent on the chain length of the fluorinated tail. *Int. J. Cancer.* **1998**, *78*, 491−495.
13. Biegel, L.B.; Hurtt, M.E.; Frame, S.R.; Connor, J. O.; Cook, J.C. Mechanisms of extrahepatic tumor induction by peroxisome proliferators in male CD rats. *Toxicol. Sci.* 2001, *60*, 44−55.
14. Jackson, D.A.; Young, C.J.; Hurley, M.D.; Wallington, T.J.; Mabury, S.A. Atmospheric degradation of perfluoro-2-methyl-3-pentanone: Photolysis, hydrolysis and hydration. *Environ Sci. Technol.* **2011**, *45*, 8030−8036.
15. Scott, B.F.; Spencer, C.; Mabury, S.A.; Muir, D.C.G. Environ. Poly and perfluorinated carboxylates in North American precipitation. *Sci. Technol.* **2006**, *40*, 7167−7174.
16. Young, C.J.; Hurley, M.l.D.; Wallington, T.J.; Mabury, S.A. Atmospheric chemistry of CF₃CF₂H and CF₃CF₂CF₂CF₂H: Kinetics and products of gas-phase reactions with Cl atoms and OH radicals, infrared spectra, and formation of perfluorocarboxylic acids. *Chem. Phys. Lett.* **2009**, *473*, 251−256.
17. Grubbs, G.S. II; Obenchain, D.A.; Frank, D.S.; Novick, S.E.; Cooke, S.A.; Serrato, A. III; Lin W. A study of the monohydrate and dihydrate complexes of perfluoropropionic acid using Chirped-Pulse Fourier Transform Microwave (CP-FTMW) spectroscopy. *J Phys Chem A.* **2015**, *119(42)*, 10475−80.
18. Crowder, G.A. Infrared and Raman spectra of pentafluoropropionic acid. *J. Fluorine Chem*. **1972**, *1(4)*, 385−389.
19. Kagarise, R.E. Relation between the electronegativities of adjacent substitutents and the stretching frequency of the carbonyl group, *J. Am. Chem. Soc.***1955**, *77(5),* 1377−1379.

20. Statz, G.; Lippert, E. Far infrared spectroscopic studies on carboxylic acid solutions, *Ber. Bunsen-Ges.*, **1967**, *71(7)*, 673–679.

21. Badawi, H. M.; Al-Khaldi, M. A. A.; Al-Sunaidi, Z. H. A.; Al-Abbad, S. S. A. Conformational properties and vibrational analyses of monomeric pentafluoropropionic acid CF_3CF_2COOH and pentafluoropropionamide $CF_3CF_2CONH_2$, *Can. J. Anal. Sci. Spectrosc.* **2007**, *52(5)*, 252–269.

22. Grubbs, G.S. II; Serrato, A. III; Obenchain, Cooke, S.A.; D.A.; Frank, D.S.; Novick, S.E.; Lin W. The rotational spectrum of perfluoropropionic acid, *J. Mol. Spectrosc.* **2012**, *275*, 1–4.

23. Husted D.R.; Ahlbrecht A.H. The chemistry of the perfluoro acids and their derivatives. V. Perfluoropropionic acid, *J. Am. Chem. Soc.* **1953**, *75(7)*, 1605–1608.

24. Collins M.F.; Haywood B.C. Vibration spectra of carboxylic acids by neutron spectroscopy, *J. Chem. Phys.* **1970**, *52*, 5740–5745.

25. Rontu, N.; Vaida V. Vibrational spectroscopy of perfluorocarboxylic acids from the infrared to the visible regions, *J. Phys. Chem. B* **2008**, *112*, 276–282.

26. Rontu, N.; Vaida V. Vibrational spectroscopy of perfluoropropionic acid in the region between 1000 and 11000 cm^{-1}, *J. Mol. Spectros.* **2006**, *237*, 19–26.

27. Cho, S.; Remucal, C.K.; We,i H. Common and distinctive Raman spectral features for the identification and differentiation of per- and polyfluoroalkyl substances. *ACS EST Water* **2025**, *5(1)*, 300–309.

28. Lee E.; Featherstone, J.; Martens, J.; McMahon T.B.; Hopkins; W.S. Fluorinated propionic acids unmasked: Puzzling fragmentation phenomena of the deprotonated species, *J. Phys. Chem. Lett.* **2024**, *15*, 3029−3036.

29. Berrueta Martínez, Y.; Bava Y.B.; Cavasso Filho R.L.; Erben M.F.; Romano R.M.; Della Védova C.O. Valence and inner electronic excitation, ionization, and fragmentation of perfluoropropionic acid, *J. Phys. Chem. A* **2018**, *122*, 9842−9850.

30. Litvanová, K.; Klemetsrud, B.; Xiao F.; Kubátová A. Investigation of real-time gaseous thermal decomposition products of representative per- and polyfluoroalkyl substances (PFAS), *J. Am. Soc. Mass Spectrom.* **2025**, *36*, 108−118.

31. Wiens, J.P.; Miller; T.H., Ard, S.G.; Viggiano, A.A.; Shuman, N.S. Elementary reactions leading to perfluoroalkyl substance degradation in an Ar^+/e^- Plasma, *J. Phys. Chem. A* **2022**, *126*, 9076−9086.

32. Wang, W.; Song, M.; Abusallout, I.; Hanigan, D. Thermal decomposition of two gaseous perfluorocarboxylic acids: Products and mechanisms. *Environ. Sci. Technol.* **2023**, *57*, 6179−6187.

33. Melin, T.R.L.; Harell, P.; Ali, B; Loganathan, N.; Wilson A.K. Thermochemistry of per- and polyfluoroalkyl substances. *J Comput Chem.* **2023**, *44*, 570–580.

34. Medeiros F.S. Jr.; Jr.; Mota C.; Chaudhuri, P. Perfluoropropionic acid-driven nucleation of atmospheric molecules under ambient conditions. *J. Phys. Chem. A* **2022**, *126*, 8449−8458.

35. Sablinskas, V.; Pucetaite, M.; Ceponkus, J.; Kimtys L. Structure of propanoic acid dimers as studied by means of MIR and FIR spectroscopy. *J. Mol. Struct.* **2010**, *976(1–3)*, 263−269.

36. Alvarez, S. A cartography of the van der Waals territories. *Dalton Trans*. **2013**, *42*, 8617–8636.

37. Frisch, M.J.; Trucks, G.W.; Schlegel, H.B.; Scuseria, G.E.; Robb, M.A.; Cheeseman, J.R.; Montgomery, J.A. Jr.; Vreven, T.; Kudin, K.N.; Burant, J.C.; Millam, J.M.; Iyengar, S.S.; et al. Gaussian 03, rev C.02; Gaussian, Inc., Wallingford CT, 2004.

38. Parr, R.G.; Yang, W. Density-Functional Theory of atoms and molecules; *Oxford University Press: USA*, **1989**.

39. Møller, C.; Plesset, M.S. Note on an approximation treatment for many-electron systems, *Phys. Rev.* **1934**, *46*, 618–622.

40. Foster, J.P; Weinhold, F. Natural hybrid orbitals. *J. Am. Chem. Soc.* **1980**, *102*, 7211–7218.

41. Glendening, E.D.; Badenhoop, J.K.; Reed, A.E.; Carpenter, J.E;. Bohmann, J.A.; Morales, C.M.; Weinhold F. NBO 5.G, Theoretical Chemistry Institute, University of Wisconsin, Madison, WI 2004.

42. Almond, M. J.; Downs, A. J. Spectroscopy of matrix isolated species. *Adv. Spectrosc*. **1989**, *17*, 1–505.

43. Dunkin, I.R. Matrix-Isolation Techniques: A Practical Approach; *Oxford University Press*: New York, 1998.

44. Perutz, R. N.; Turner, J. J. Pulsed matrix isolation. A comparative study. *J. Chem. Soc., Faraday Trans. 2.* **1973**, *69*, 452–461.

45. Dolomanov, O.V.; Bourhis, L.J.; Gildea, R.J.; Howard, J.A.K.; Puschmann, H. OLEX2: a complete structure solution, refinement and analysis program. *J. Appl. Cryst.* **2009,** *42*, 339–341.

46.   Sheldrick, G. M. A short history of SHELX. *Acta Cryst.* **2008,** *A64*, 112–122.

47.   Bourhis, L.J., Dolomanov, O.V., Gildea, R.J., Howard, J.A.K., Puschmann, H. The anatomy of a comprehensive constrained, restrained refinement program for the modern computing environment - Olex2 dissected, *Acta Crystallogr.* **2015**, *A71*, 59-75.

48.   Kleemiss, F., Dolomanov, O.V., Bodensteiner, M., Peyerimhoff, N., Midgley, L., Bourhis, L.J., Genoni, A., Malaspina, L.A., Jayatilaka, D., Spencer, J.L., White, F., Grundkoetter-Stock, B., Steinhauer, S., Lentz, D., Puschmann, H., Grabowsky, S, Accurate crystal structures and chemical properties from NoSpherA2, *Chem. Sci.,* **2021**, *12*, 1675–1692.

49.   Hogg, P.J. *Trends Biochem. Sci.* **2003**, *28(4),* 210–214.

50.   Hilal, R.; El-Aaser A.M. A comparative quantum chemical study of methyl acetate and S-methyl thioacetate Toward an understanding of the biochemical reactivity of esters of coenzyme A. *Biophys. Chem.* **1985,** *2*, 145–150.

51.   Beck, I.T.; Mitchell, E.C.; Webb Hill, A.; Turney, J.M; Rotavera, B.; Schaefer III, H.F. Evaluating the importance of conformers for understanding the vacuum-ultraviolet spectra of oxiranes: Experiment and theory, *J. Phys. Chem. A* **2024**, *128*, 50, 10906–10920.